

# Analysis of the optical conductivity for $A_2\text{IrO}_3$ ( $A = \text{Na}, \text{Li}$ ) from first principles

Ying Li,<sup>1</sup> Kateryna Foyevtsova,<sup>2</sup> Harald O. Jeschke,<sup>1</sup> and Roser Valentí<sup>1</sup>

<sup>1</sup>*Institut für Theoretische Physik, Goethe-Universität Frankfurt,  
Max-von-Laue-Strasse 1, 60438 Frankfurt am Main, Germany*

<sup>2</sup>*Quantum Matter Institute, University of British Columbia, Vancouver, British Columbia V6T 1Z4, Canada*  
(Dated: June 28, 2021)

We present results for the optical conductivity of  $\text{Na}_2\text{IrO}_3$  within density functional theory by including spin-orbit (SO) and correlation effects (U) as implemented in GGA+SO+U. We identify the various interband transitions and show that the underlying quasi-molecular-orbital nature of the electronic structure in  $\text{Na}_2\text{IrO}_3$  translates into distinct features in the optical conductivity. Most importantly, the parity of the quasi-molecular orbitals appears to be the main factor in determining strong and weak optical transitions. We also present optical conductivity calculations for  $\text{Li}_2\text{IrO}_3$  and discuss the similarities and differences with  $\text{Na}_2\text{IrO}_3$ .

The family of honeycomb iridates  $A_2\text{IrO}_3$  ( $A = \text{Na}, \text{Li}$ ) has recently been a subject of intensive discussion due to its complex electronic and magnetic behavior arising from an interplay of spin-orbit effects, correlations and lattice geometry. These materials are insulators and order antiferromagnetically at low temperatures<sup>1</sup>. While  $\text{Na}_2\text{IrO}_3$  shows a zigzag-like magnetic pattern<sup>2</sup>, a spiral order with a small nonzero wave vector inside the first Brillouin zone has been reported for  $\text{Li}_2\text{IrO}_3$ <sup>3,4</sup>. Photoemission and optical conductivity measurements<sup>5</sup> for  $\text{Na}_2\text{IrO}_3$  confirm this insulating behavior with a gap of 340 meV. Attempts to understand the different behavior of the end members through the series  $(\text{Na}_{1-x}\text{Li}_x)_2\text{IrO}_3$  have been pursued<sup>6,7</sup> with partly contradicting results, while Manni *et al.*<sup>6</sup> find that only for  $x \leq 0.25$  does the system form uniform solid solutions and otherwise the system shows a miscibility gap and phase separates, Cao *et al.*<sup>7</sup> report a homogeneous phase at  $x \sim 0.7$  with a disappearance of long range magnetic order.

From a theoretical point of view, these materials have been suggested to be a realization of the Heisenberg-Kitaev model with bond-dependent anisotropic interactions between  $j_{\text{eff}} = 1/2$  spin-orbit-coupled Ir moments<sup>8–13</sup>. Such a model is obtained under the assumption of large spin-orbit coupling, so that Ir 5d  $t_{2g}$  orbitals can be written in terms of  $j_{\text{eff}} = 1/2$  and lower lying  $j_{\text{eff}} = 3/2$  relativistic orbitals.

Alternatively, a description of the electronic structure of these systems in terms of quasi-molecular orbitals was also recently proposed<sup>14,15</sup>. Following the observation that the contributing energy scales in these systems are of the same order of magnitude, namely the bandwidth for 5d orbitals is 1.5-2 eV, the onsite Coulomb repulsion U is about 1-2 eV, the Hund's coupling constant is about 0.5 eV and the spin-orbit coupling is  $\lambda \sim 0.4$ -0.5 eV it was shown<sup>14,15</sup> that the underlying electronic behavior can be described in terms of molecular orbitals formed by the Ir  $t_{2g}$  states on an hexagon with each of the three  $t_{2g}$  Ir orbitals on a site contributing to three neighboring molecular orbitals. In Ref. 15 it was further demonstrated that both descriptions, i.e. a localized description in terms of  $j_{\text{eff}}$  and an itinerant description in terms of molecular orbitals are equally compatible.

Presently, only optical conductivity  $\sigma(\omega)$  measurements for  $\text{Na}_2\text{IrO}_3$  are available<sup>5,16</sup>.  $\sigma(\omega)$  in  $\text{Na}_2\text{IrO}_3$  shows a broad peak structure at 1.5 eV<sup>5</sup> (1.66 eV in Ref. 16) and smaller peak structures at 0.52 eV, 0.72 eV, 1.32 eV, 1.98 eV<sup>16</sup>. These features have been interpreted in terms of dominant  $j_{\text{eff}} = 3/2$  and  $j_{\text{eff}} = 1/2$  transitions<sup>16</sup>. With the aim of further unveiling the origin of different behavior in  $\text{Na}_2\text{IrO}_3$  and  $\text{Li}_2\text{IrO}_3$ , we revisit the optical conductivity in  $\text{Na}_2\text{IrO}_3$  with density functional theory calculations and show that the nature of the various interband transitions observed experimentally can be understood in terms of the parity of the underlying molecular orbital description. In contrast, the optical conductivity behavior that we predict for  $\text{Li}_2\text{IrO}_3$  shows an increase in weight at low energies with respect to  $\text{Na}_2\text{IrO}_3$  due to a strong mixing of quasi-molecular orbital character, absent in  $\text{Na}_2\text{IrO}_3$ .

For our density functional theory (DFT) calculations we use the full-potential linearized augmented plane-wave (LAPW) method as implemented in the code WIEN2k<sup>17</sup>. The PBE generalized gradient approximation (GGA)<sup>18</sup> was employed as exchange correlation functional and the basis-size controlling parameter  $RK_{\text{max}}$  was set to 8. A mesh of 450 **k** points in the first Brillouin zone (FBZ) for the self-consistency cycle was used. In order to have a good description of the experimentally observed optical gap in  $\text{Na}_2\text{IrO}_3$ , magnetism as well as a  $U_{\text{eff}} = 2.4$  eV as implemented in GGA+U<sup>19</sup> had to be included in the calculations. Relativistic effects were taken into account within the second variational approximation (GGA+SO+U). For the optical properties, we employed the optics code package<sup>20</sup> in WIEN2k. The optical properties were calculated with 1568 **k** points in the FBZ.

The imaginary part of the interband contribution to the dielectric function is given by<sup>20,21</sup>:

$$\text{Im}\epsilon_{\alpha\beta}(\omega) \propto \frac{1}{\omega^2} \sum_{c,v} \int d\mathbf{k} \langle c_{\mathbf{k}} | p^\alpha | v_{\mathbf{k}} \rangle \langle v_{\mathbf{k}} | p^\beta | c_{\mathbf{k}} \rangle \times \delta(\epsilon_{c_{\mathbf{k}}} - \epsilon_{v_{\mathbf{k}}} - \omega). \quad (1)$$

Here,  $\alpha$  and  $\beta$  indicate directional components,  $p$  is the momentum operator, and  $\omega$  corresponds to the energy of the photon.  $c_{\mathbf{k}}$  denotes a state in the conduction band

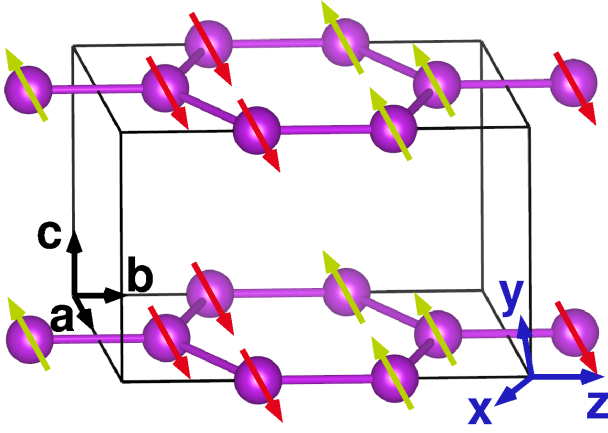


FIG. 1: (Color online) Ir honeycomb layers of  $\text{Na}_2\text{IrO}_3$ . The black axis  $\mathbf{a}$ ,  $\mathbf{b}$ , and  $\mathbf{c}$  are the vectors of the unit cell, while the dark blue axes  $\mathbf{x}$ ,  $\mathbf{y}$ ,  $\mathbf{z}$  are the Cartesian axes. The red and green arrows show the zigzag AFM phase.

with the energy  $\varepsilon_{c\mathbf{k}}$  and  $v_{\mathbf{k}}$  is a state in the valence band with the energy  $\varepsilon_{v\mathbf{k}}$ . By absorbing photon energy, the electrons transit from  $v_{\mathbf{k}}$  to  $c_{\mathbf{k}}$ . The real part of the dielectric function can be evaluated from the imaginary part using the Kramers-Kronig relation. In this work we focus on the analysis of the real part of the optical conductivity

$$\text{Re } \sigma_{\alpha\beta}(\omega) = \frac{\omega}{4\pi} \text{Im } \epsilon_{\alpha\beta}(\omega). \quad (2)$$

For our DFT analysis we used the experimental structure of  $\text{Na}_2\text{IrO}_3$  given in Ref. 2 which agrees well with the relaxed structure<sup>2,6</sup> and performed GGA+SO+U ( $U = 3$  eV,  $J_{\text{H}} = 0.6$  eV,  $U_{\text{eff}} = U - J_{\text{H}} = 2.4$  eV) calculations in the zigzag antiferromagnetic (AFM) ordered phase (see Fig. 1) with the magnetization parallel to the  $\mathbf{a}$  direction<sup>22</sup>.

The density of states (DOS) and band structures for  $\text{Na}_2\text{IrO}_3$  within GGA, GGA+SO, and GGA+SO+U are shown in Fig. 2. Compared to the non-relativistic GGA DOS, a suppression of the DOS at  $E_{\text{F}}$  is clearly visible in the relativistic GGA+SO calculation. In GGA+SO+U, a 341 meV gap can be obtained as reported experimentally<sup>5</sup>. Note that in the zigzag AFM phase there are 4 iridium atoms per unit cell and therefore the number of bands doubles to 12  $t_{2g}$  in Fig. 2.

The monoclinic symmetry allows for four independent components of the optical conductivity tensor defined as  $\sigma_{xx}$ ,  $\sigma_{yy}$ ,  $\sigma_{zz}$ ,  $\sigma_{xy}$

$$\begin{pmatrix} J_x \\ J_y \\ J_z \end{pmatrix} = \begin{pmatrix} \sigma_{xx} & \sigma_{xy} & 0 \\ \sigma_{xy} & \sigma_{yy} & 0 \\ 0 & 0 & \sigma_{zz} \end{pmatrix} \begin{pmatrix} E_x \\ E_y \\ E_z \end{pmatrix}. \quad (3)$$

The Cartesian directions are shown in Fig. 1.  $\mathbf{z}$  is parallel to the  $\mathbf{b}$  direction and lies in the Ir hexagonal plane, while  $\mathbf{x}$  and  $\mathbf{y}$  are in the  $ac$  plane. Spin-orbit coupling also induces small non-zero contributions to the  $\sigma_{xz}$  and  $\sigma_{yz}$  components.

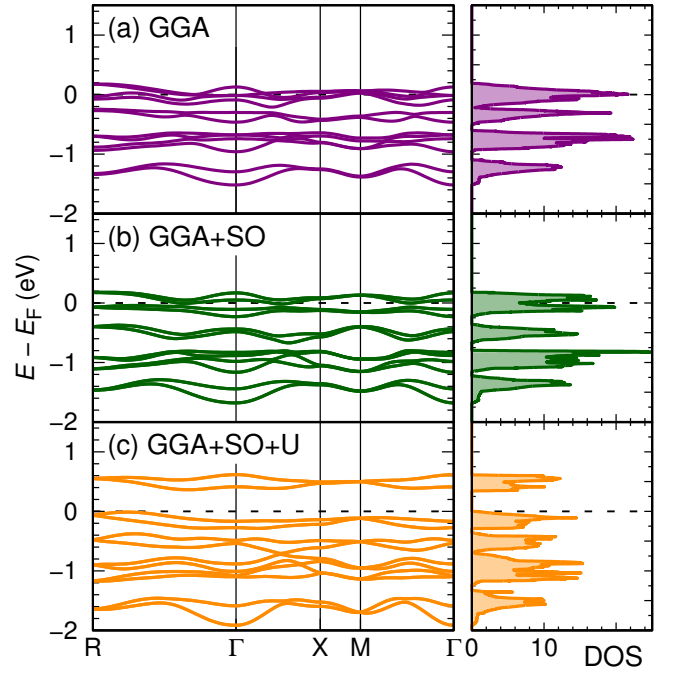


FIG. 2: (Color online) Ir 5d  $t_{2g}$  DOS and band structures for  $\text{Na}_2\text{IrO}_3$ , obtained with (a) GGA, (b) GGA+SO, and (c) GGA+SO+U ( $U=3$  eV,  $J_{\text{H}}=0.6$  eV,  $U_{\text{eff}} = U - J_{\text{H}} = 2.4$  eV).

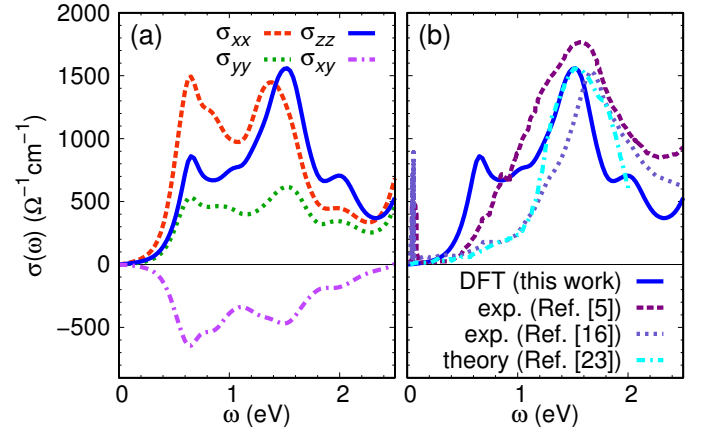


FIG. 3: (Color online) (a) Optical conductivity tensor components  $\sigma_{xx}$ ,  $\sigma_{yy}$ ,  $\sigma_{zz}$ ,  $\sigma_{xy}$  and (b) DFT  $\sigma_{zz}$  for  $\text{Na}_2\text{IrO}_3$  compared with experiment<sup>5,16</sup> and theory data<sup>23</sup>.

In Fig. 3 (a), we present the calculated four dominant optical conductivity tensor components for  $\text{Na}_2\text{IrO}_3$  in the low-frequency region. Only  $\sigma_{zz}$  corresponds to the in-plane optical conductivity and in Fig. 3 (b) we compare this component with the experimental results<sup>5,16</sup> as well as with a 4-site iridium cluster calculations by Kim *et al.*<sup>23</sup>. Both, our DFT calculations and the cluster calculations<sup>23</sup> show the presence of a dominant peak at  $\omega = 1.5$  eV as observed in experiment. However, the DFT results have a richer structure and capture the multi-peak behavior of the experimental observations.

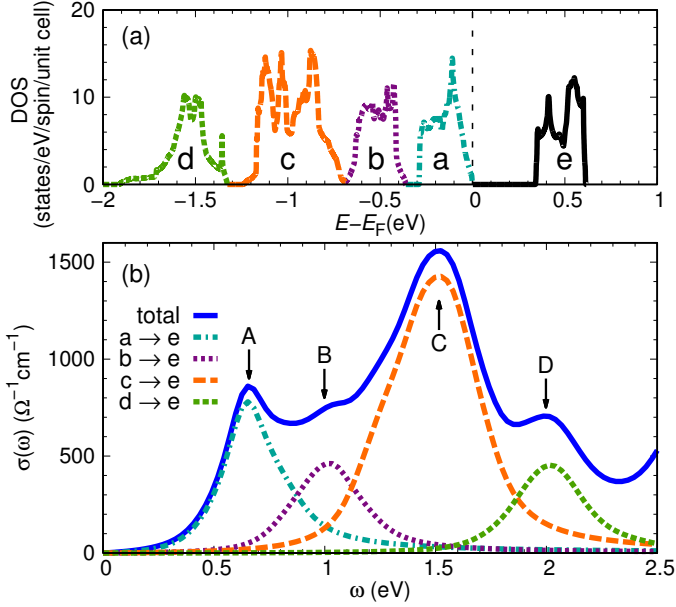


FIG. 4: (Color online) GGA+SO+U density of states (a) and contributions from different  $d$ - $d$  transitions (b). The a, b, c, d, e label the 5 states.

In order to disentangle the origin of the various features present in the optical conductivity in Fig. 3 (b), we display in Fig. 4 the various interband processes. For that purpose, we label in Fig. 4 (a) the valence states  $v_s$  as a, b, c, d and the conduction states  $c_s$  as e. We identify four peaks in  $\sigma(\omega)$  (Fig. 4 (b)); peaks A, B, C, D correspond to the transitions from a, b, c, d to e states, respectively. The analysis of the electronic structure in terms of quasi-molecular orbitals<sup>14,15</sup> predicts a clear odd/even parity related to the symmetry of the quasi-molecular orbitals, i.e. odd  $B_{1u}$ , even  $E_{1g}$ , odd  $E_{2u}$  and even  $A_{1g}$ . Even though the zigzag magnetic order used for the calculations mixes states of different parities, we find in our analysis of the magnetic quasi-molecular orbitals that the dominating parity contribution to a given state matches the parity of this state's counterpart in the paramagnetic phase. This, in particular, allows us to compare our spin-polarized calculations with the measurements performed above the magnetic transition temperature.

In the GGA+SO+U calculations we find that the states a, b, c, d, and e are predominantly of even, odd, even, odd, and odd parity, respectively; note that in the presence of spin-orbit coupling the states from the upper triad cannot be identified in terms of quasi-molecular orbitals, however we can still discern the dominant parity. Since the dielectric tensor matrix elements involved in the optical interband transitions are of the form  $\langle v_s | \mathbf{E} \cdot \mathbf{r} | c_s \rangle$  with  $\mathbf{E} \cdot \mathbf{r}$  being an odd parity operator, clearly, transitions between states of the same parity will be strongly suppressed whereas transitions between states of different parity will dominate. This is reflected in the large peak at 1.5 eV (peak C) that corresponds to a predomi-

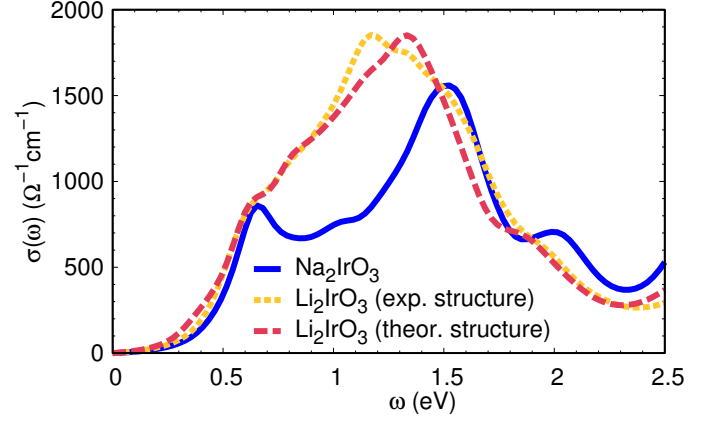


FIG. 5: (Color online) Comparison of the optical conductivity  $\sigma_{zz}$  between  $\text{Na}_2\text{IrO}_3$  (experimental structure) and  $\text{Li}_2\text{IrO}_3$  (experimental and theoretically predicted structure).

nantly even to odd parity transition, followed by peak A (predominantly even to odd), while peaks B and D are of transitions between predominantly equal (odd) parity states and are strongly suppressed (see Ref. 14, Supplement). The optical conductivity is therefore an important measure of the underlying molecular orbital structure in  $\text{Na}_2\text{IrO}_3$ .

We now proceed with the calculation of the optical conductivity for  $\text{Li}_2\text{IrO}_3$ . The  $\text{Li}_2\text{IrO}_3$  structure is known from powder x-ray diffraction<sup>24</sup> and from a careful DFT structure prediction using a spin-polarized GGA+SO+U exchange correlation functional<sup>6</sup>. As these two structures differ slightly and also show small but significant differences in electronic structure<sup>25</sup>, we determine the optical conductivity for both of them. Experiments indicate that the gap of  $\text{Li}_2\text{IrO}_3$  is of the same order of magnitude as in  $\text{Na}_2\text{IrO}_3$ <sup>24</sup> or a bit smaller<sup>26</sup>. We find that magnetism and a  $U_{\text{eff}} = 2.4$  eV are necessary to open a gap of about 318 meV for the experimental structure while  $U_{\text{eff}} = 2.0$  eV is necessary to open a gap of about 307 meV for the theoretical structure. Even though a spiral order has been suggested from experiment<sup>3</sup>, we have considered, for simplicity, a zigzag magnetic order as in  $\text{Na}_2\text{IrO}_3$  for the calculations.

We compare the optical conductivities of  $\text{Na}_2\text{IrO}_3$  and  $\text{Li}_2\text{IrO}_3$  in Figure 5. While the dominant peak in the  $\text{Na}_2\text{IrO}_3$  optical conductivity is at 1.5 eV, we find it at 1.17 eV for the experimental structure and at 1.33 eV for the theoretical structure of  $\text{Li}_2\text{IrO}_3$ . Also, we observe an increase of the optical conductivity weight between 0.66 eV and 1.48 eV with respect to  $\text{Na}_2\text{IrO}_3$ . In order to analyze this behavior, we project the nonmagnetic GGA electronic structure of  $\text{Li}_2\text{IrO}_3$  onto the quasi-molecular orbital basis (see Fig. 6). We observe that the separation of the density of states into isolated narrow bands of unique quasi-molecular orbital characters is much less clean than in  $\text{Na}_2\text{IrO}_3$ <sup>14,15</sup> and resembles the case of  $\text{Li}_2\text{RhO}_3$ <sup>27</sup>. In  $\text{Li}_2\text{IrO}_3$ , there is overlapping between  $B_{1u}$

and  $E_{1g}$  states and between  $E_{1g}$  and  $A_{1g}/E_{2u}$  states as shown in Fig. 6. This strong mixing of character, which remains in the magnetic calculations, explains why the B peak in  $\text{Li}_2\text{IrO}_3$  is much stronger than in  $\text{Na}_2\text{IrO}_3$ ; the suppressed odd to odd transition in  $\text{Na}_2\text{IrO}_3$  evolves into a mixture of enhanced and suppressed transitions in  $\text{Li}_2\text{IrO}_3$ .

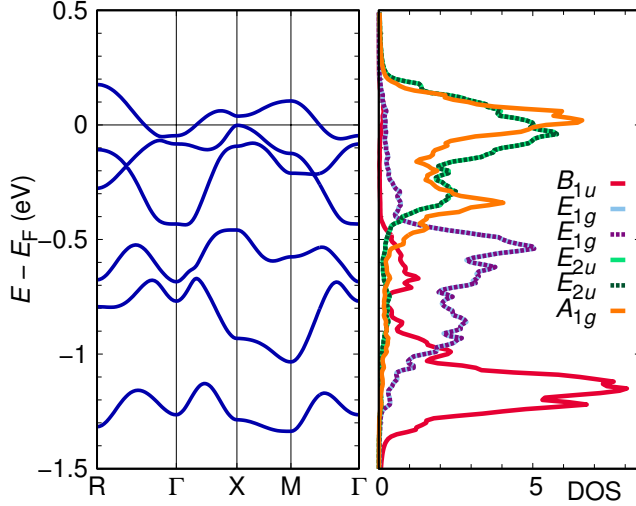


FIG. 6: (Color online) Nonrelativistic nonmagnetic band structure and density of states of the theoretically predicted  $\text{Li}_2\text{IrO}_3$  structure, projected onto quasi-molecular orbitals.

We would like to emphasize that all above DFT calculations have been performed with inclusion of spin-orbit effects, and, strictly speaking, neither the  $t_{2g}$  (or the lin-

ear combination of  $t_{2g}$  states forming quasi-molecular orbitals) nor spin are well defined entities. Nevertheless, we have shown that the main features observed in optical conductivity are related to the underlying symmetries of the molecular orbital basis, which is a manifestation of the fact that spin-orbit coupling is not the only determining interaction in these materials.

In summary, we have investigated the optical conductivity in  $\text{Na}_2\text{IrO}_3$  and  $\text{Li}_2\text{IrO}_3$  by performing magnetic GGA+SO+U calculations. Magnetism and a nonzero  $U$  were necessary in order to reproduce the experimental insulating gap in both systems. Using the fact that the narrow bands of  $\text{Na}_2\text{IrO}_3$  are well described in terms of quasi-molecular orbitals, we showed that the strength of the various interband contributions to the optical conductivity can be well described in terms of the parity of the quasi-molecular orbitals, namely weight suppression in like-parity transitions and weight enhancement in unlike-parity transitions. We also predict the shape of the optical conductivity for  $\text{Li}_2\text{IrO}_3$ . Contrary to  $\text{Na}_2\text{IrO}_3$ , in  $\text{Li}_2\text{IrO}_3$  the quasi-molecular orbitals strongly overlap and parities mix. This explains the relative weight differences in the optical conductivity between  $\text{Li}_2\text{IrO}_3$  and  $\text{Na}_2\text{IrO}_3$ .

#### Acknowledgments

We would like to thank J. Orenstein, R. Coldea, J. Analytis, X. Xi, I. I. Mazin and G. Khaliullin for very useful discussions. Y.L. acknowledges support through a China Scholarship Council (CSC) Fellowship. H.O.J. and R.V. acknowledge support by the Deutsche Forschungsgemeinschaft through grant SFB/TR 49.

- <sup>1</sup> Y. Singh and P. Gegenwart, Phys. Rev. B **82**, 064412 (2010).
- <sup>2</sup> S. K. Choi, R. Coldea, A. N. Kolmogorov, T. Lancaster, I. I. Mazin, S. J. Blundell, P. G. Radaelli, Y. Singh, P. Gegenwart, K. R. Choi, S.-W. Cheong, P. J. Baker, C. Stock, and J. Taylor, Phys. Rev. Lett. **108**, 127204 (2012).
- <sup>3</sup> R. Coldea, presentation at the MPI-Dresden workshop on Spin-Orbit Entanglement (July 2013).
- <sup>4</sup> I. Kimchi, R. Coldea, A. Vishwanath, arXiv:1408.3640
- <sup>5</sup> R. Comin, G. Levy, B. Ludbrook, Z.-H. Zhu, C. N. Veenstra, J. A. Rosen, Y. Singh, P. Gegenwart, D. Stricker, J. N. Hancock, D. van der Marel, I. S. Elfimov, and A. Damascelli, Phys. Rev. Lett. **109**, 266406 (2012).
- <sup>6</sup> S. Manni, S. Choi, I. I. Mazin, R. Coldea, M. Altmeyer, H. O. Jeschke, R. Valentí, and P. Gegenwart, Phys. Rev. B **89**, 245113 (2014).
- <sup>7</sup> G. Cao, T. F. Qi, L. Li, J. Terzic, V. S. Cao, S. J. Yuan, M. Tovar, G. Murthy, R. K. Kaul, Phys. Rev. B **88**, 220414 (2013).
- <sup>8</sup> J. Chaloupka, G. Jackeli, and G. Khaliullin, Phys. Rev. Lett. **105**, 027204 (2010).
- <sup>9</sup> Y. Yamaji, Y. Nomura, M. Kurita, R. Arita, and M. Imada, Phys. Rev. Lett. **113**, 107201 (2014).
- <sup>10</sup> V. M. Katukuri, S. Nishimoto, V. Yushankhai, A. Stoy-

- anova, H. Kandpal, S. Choi, R. Coldea, I. Rousochatzakis, L. Hozoi, J. van den Brink New J. Phys. **16**, 013056 (2014).
- <sup>11</sup> J. G. Rau, E. K.-H. Lee, H.-Y. Kee, Phys. Rev. Lett. **112**, 077204 (2014).
- <sup>12</sup> J. Reuther, R. Thomale, S. Rachel, Phys. Rev. B **90**, 100405(R) (2014).
- <sup>13</sup> Y. Szyzyk, C. Price, P. Wölfle, N. B. Perkins, arXiv:1408.3647.
- <sup>14</sup> I. I. Mazin, H. O. Jeschke, K. Foyevtsova, R. Valentí, and D. I. Khomskii, Phys. Rev. Lett. **109**, 197201 (2012).
- <sup>15</sup> K. Foyevtsova, H. O. Jeschke, I. I. Mazin, D. I. Khomskii, and Roser Valentí, Phys. Rev. B **88**, 035107 (2013).
- <sup>16</sup> C. H. Sohn, H.-S. Kim, T. F. Qi, D. W. Jeong, H. J. Park, H. K. Yoo, H. H. Kim, J.-Y. Kim, T. D. Kang, Deok-Yong Cho, G. Cao, J. Yu, S. J. Moon, and T. W. Noh, Phys. Rev. B **88**, 085125 (2013).
- <sup>17</sup> P. Blaha, K. Schwarz, G. K. H. Madsen, D. Kvasnicka, J. Luitz, WIEN2k, *An Augmented Plane Wave + Local Orbitals Program for Calculating Crystal Properties* (Karlheinz Schwarz, Techn. Universität Wien, Austria, 2001).
- <sup>18</sup> J. P. Perdew, K. Burke, and M. Ernzerhof, Phys. Rev. Lett. **77**, 3865 (1996).
- <sup>19</sup> V. I. Anisimov, I. V. Solovyev, M. A. Korotin, M. T. Czyzyk, and G. A. Sawatzky, Phys. Rev. B **48**, 16929

- (1993).
- <sup>20</sup> C. Ambrosch-Draxl and J. O. Sofo, *Comput. Phys. Commun.* **175**, 1 (2006).
- <sup>21</sup> J. Ferber, Y.-Z. Zhang, H. O. Jeschke, and R. Valenti, *Phys. Rev. B* **82**, 165102 (2010).
- <sup>22</sup> X. Liu, T. Berlijn, W.-G. Yin, W. Ku, A. Tsvelik, Y.-J. Kim, H. Gretarsson, Y. Singh, P. Gegenwart, and J. P. Hill, *Phys. Rev. B* **83**, 220403(R) (2011).
- <sup>23</sup> B. H. Kim, G. Khaliullin, and B. I. Min, *Phys. Rev. B* **89**, 081109(R) (2014).
- <sup>24</sup> H. Gretarsson, J. P. Clancy, X. Liu, J. P. Hill, E. Bozin, Y. Singh, S. Manni, P. Gegenwart, Jungho Kim, A. H. Said, D. Casa, T. Gog, M. H. Upton, H.-S. Kim, J. Yu, V. M. Katukuri, L. Hozoi, J. van den Brink, and Y.-J. Kim, *Phys. Rev. Lett.* **110**, 076402 (2013).
- <sup>25</sup> See Supplementary Information.
- <sup>26</sup> M. Jenderka, R. Schmidt-Grund, M. Grundmann, and M. Lorenz, *arXiv:1407.3596*.
- <sup>27</sup> I. I. Mazin, S. Manni, K. Foyevtsova, H. O. Jeschke, P. Gegenwart, R. Valenti, *Phys. Rev. B* **88**, 035115 (2013).

## Supplementary Information

### S1. The effect of broadening

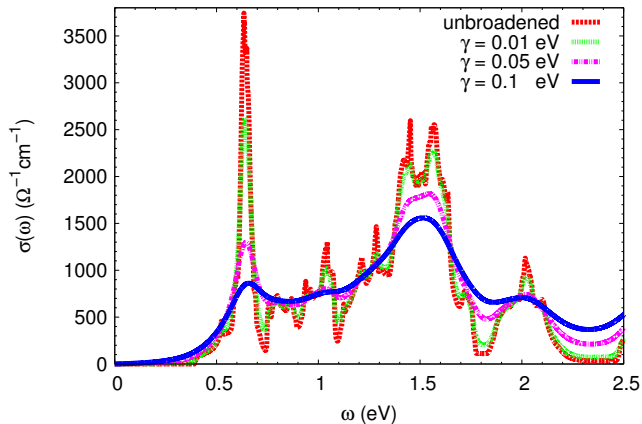


FIG. S1: (Color online) Optical conductivity for  $\text{Na}_2\text{IrO}_3$  without and with different broadenings  $\gamma = 0.01, 0.05$ , and  $0.1$  eV.

The unbroadened theoretical spectra require a substantial broadening for a meaningful comparison with the experimental data. We use different values of the Lorentzian broadening  $\gamma$  within the WIEN2k optics package to obtain the broadened theoretical spectra in Fig. S1. We choose  $\gamma = 0.1$  eV as the broadening to compare with experiment.

### S2. The electronic structure for $\text{Li}_2\text{IrO}_3$

For performing DFT calculations on  $\text{Li}_2\text{IrO}_3$ , we used the experimentally determined atomic positions and lat-

tice parameters, the latter being  $a = 5.172$  Å,  $b = 8.926$  Å,  $c = 5.122$  Å,  $\alpha = \gamma = 90^\circ$ ,  $\beta = 109.91^\circ$  (see Ref. S1). The corresponding electronic structure is shown in Figure S2 (left). We also used the crystal structure predicted in Ref. S2 with spin polarized GGA+SO+U. In this case, the lattice constants are  $a = 5.21518$  Å,  $b = 9.01171$  Å,  $c = 5.14869$  Å,  $\alpha = \gamma = 90^\circ$ ,  $\beta = 109.89^\circ$  and the electronic structure is presented in Figure S2 (right). The spin-polarized GGA+SO calculation for the theoretical structure converges to a nonmagnetic solution and the DOS is similar to that of  $\text{Na}_2\text{IrO}_3$ , which has a very low DOS at  $E_F$ .

### S3. Optical conductivity contributed by different $d-d$ transitions for $\text{Li}_2\text{IrO}_3$

We display the optical conductivity contributions from different  $d-d$  transitions for both the experimental and theoretical crystal structures of  $\text{Li}_2\text{IrO}_3$  in Figure S3. In  $\text{Li}_2\text{IrO}_3$  the transition from the b state to the e state is strongly enhanced compared to  $\text{Na}_2\text{IrO}_3$ . In  $\text{Na}_2\text{IrO}_3$  this transition was between bands of dominantly the same parity and therefore relatively strongly suppressed. In  $\text{Li}_2\text{IrO}_3$ , due to the quasi-molecular orbital overlap and parity mixing, the B peak even dominates over the A peak. The experimental structure shows similar features.

[S1] H. Gretarsson, J. P. Clancy, X. Liu, J. P. Hill, E. Bozin, Y. Singh, S. Manni, P. Gegenwart, Jungho Kim, A. H. Said, D. Casa, T. Gog, M. H. Upton, H.-S. Kim, J. Yu, V. M. Katukuri, L. Hozoi, J. van den Brink, and Y.-J. Kim, Phys. Rev. Lett. **110**, 076402 (2013).

[S2] S. Manni, S. Choi, I. I. Mazin, R. Coldea, M. Altmeyer, H. O. Jeschke, R. Valenti, and P. Gegenwart, Phys. Rev. B **89**, 245113 (2014).

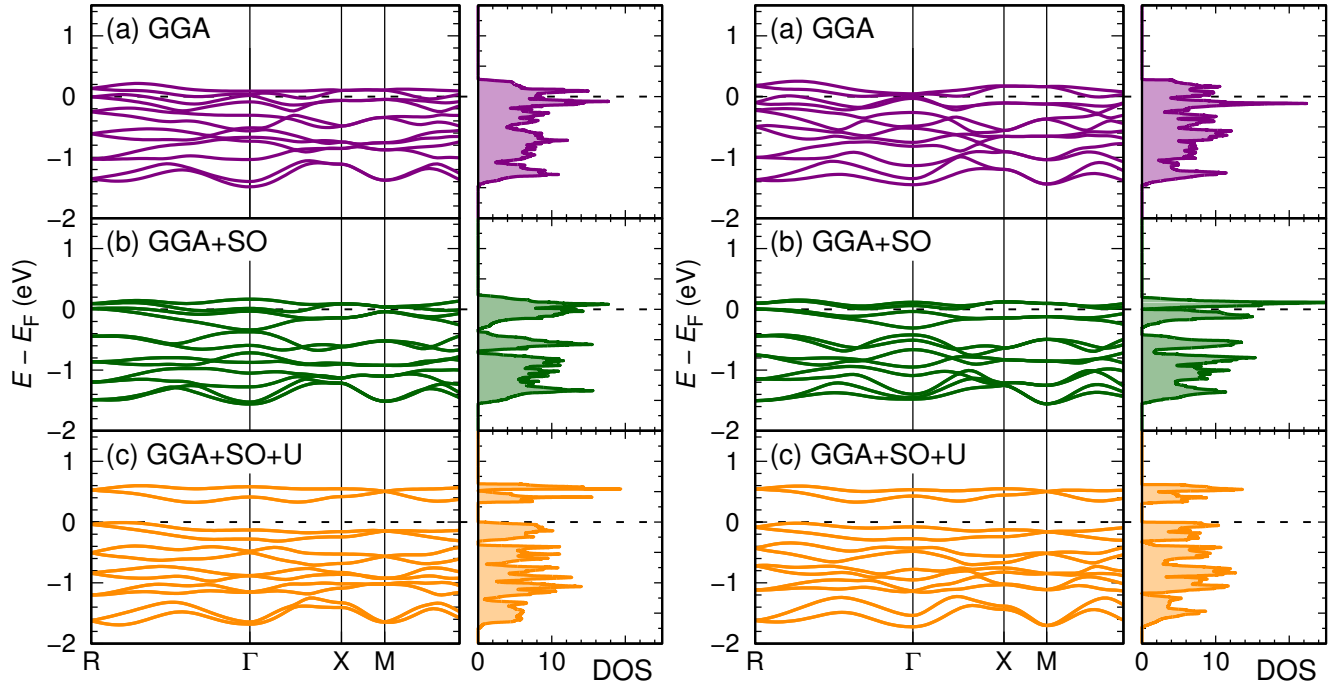


FIG. S2: (Color online) Ir 5d  $t_{2g}$  density of states and band structures for experimental  $\text{Li}_2\text{IrO}_3$  structure (left) and for the theoretical  $\text{Li}_2\text{IrO}_3$  structure (right), obtained with (a) GGA, (b) GGA+SO, and (c) GGA+SO+U.

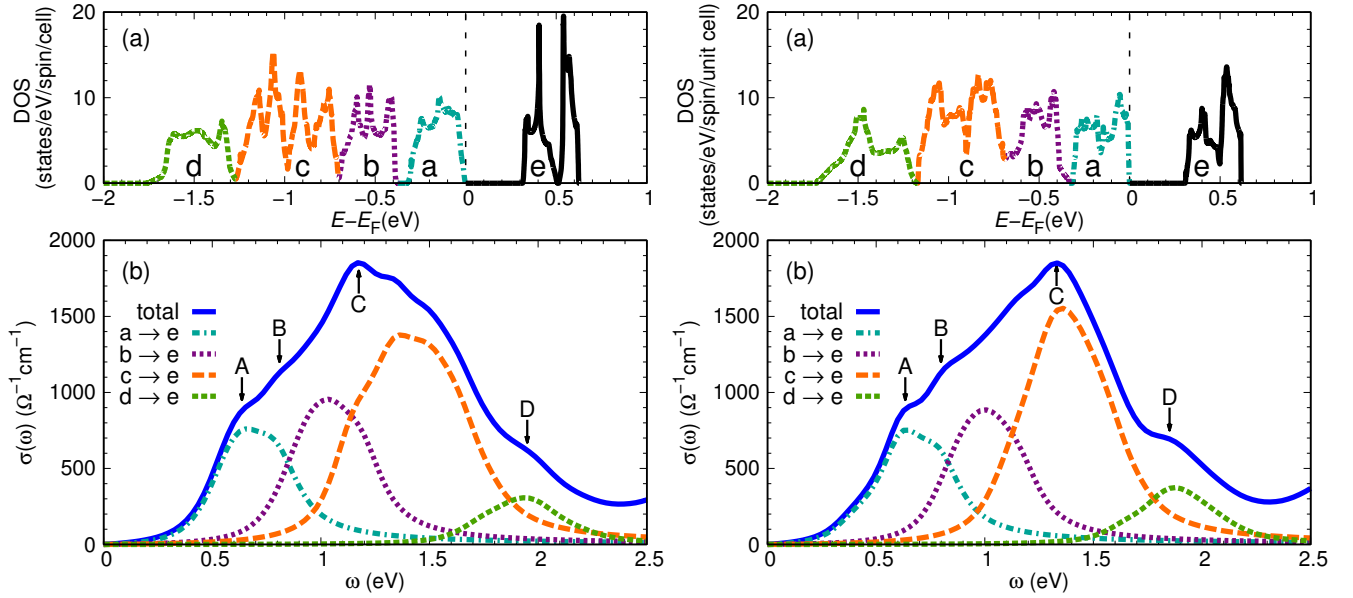


FIG. S3: (Color online) Density of states (a) and contributions from different  $d-d$  transitions (b) for the experimental  $\text{Li}_2\text{IrO}_3$  structure (left) and for the theoretical  $\text{Li}_2\text{IrO}_3$  structure (right). The a, b, c, d, e label the 5 states.